FEBS Letters 362 (1995) 156–160 FEBS 15304

# Improved measurement of $^{13}C$, $^{31}P$ J coupling constants in isotopically labeled RNA

Pascale Legault, Fiona M. Jucker, Arthur Pardi*

*Department of Chemistry and Biochemistry, University of Colorado at Boulder, Boulder, CO 80309-0215, USA*

Received 14 September 1994; revised version received 14 February 1995

**Abstract $^3J_{CP}$ coupling constants have been measured in a 99% $^{13}C$,$^{15}N$ labeled lead-dependent ribozyme, known as the leadzyme. These coupling constants were determined by analysis of the intensity of individual crosspeaks in a spin-echo difference constant time HSQC experiment. This procedure permits improved measurement of the $^3J_{C2'P}$ and $^3J_{C4'P}$ coupling constants in isotopically labeled RNA and yielded valuable information on the $\beta$ and $\epsilon$ backbone torsion angles in the leadzyme.**

*Key words:* Heteronuclear NMR; RNA structure; J coupling constant; Backbone torsion angle; Ribozyme

## 1. Introduction

Many recent studies have shown that RNAs play a central role in a variety of biological processes [1]. However, despite the increasingly important role of RNA in biology, there are still few three-dimensional structures of RNAs. NMR spectroscopy is currently the best method for determining solution structures of RNA [2]. Recent advances in synthesis of isotopically labeled RNA oligomers [3,4] have made it possible to apply heteronuclear multi-dimensional NMR techniques to the resonance assignment and structure determination of $^{13}C$,$^{15}N$ labeled RNAs [5–11]. These heteronuclear NMR techniques are revolutionizing RNA solution structure determination by allowing for more unambiguous resonance assignment [5–11] and by providing additional distance information through three- and four-dimensional NMR experiments [5,6,9]. Proton–proton distances derived from NOEs represent the primary data for generating NMR structures of biomolecules [12]. However, the relatively low density of protons in RNA, specifically in the phosphate backbone, requires that additional information be obtained for high resolution structure determination. Backbone torsion angle constraints, derived from J coupling constants, therefore represent essential data for RNA structure determination [13]. Here we present a novel application of a triple resonance spin-echo difference constant time (CT) heteronuclear single quantum correlation (HSQC) experiment [14] for quantitative measurement of $^3J_{CP}$ coupling constants in $^{13}C$ labeled RNA. This procedure was used to measure $^3J_{C4'P}$ and $^3J_{C2'P}$ coupling constants in a 99% $^{13}C$,$^{15}N$ labeled lead-dependent ribozyme known as the leadzyme [15] (see sequence in Fig. 1). We are currently using heteronuclear multi-dimensional NMR techniques to determine the three-dimensional structure of the leadzyme [16–18], and the coupling constant data presented here supply important backbone torsional angle constraints for this structure determination.

*Corresponding author. Fax: (1) (303) 492-3586.

## 2. Materials and methods

### 2.1. Sample preparation

A 99% $^{13}C$,$^{15}N$ labeled leadzyme sample was synthesized by in vitro transcription with T7 RNA polymerase using a synthetic DNA template and 99% $^{13}C$,$^{15}N$ labeled NTPs as previously described [3,19]. Note that for the experiments described the $^{15}N$ label was not required. The NMR sample was 1.2 mM RNA, 10 mM $NaPO_4$, 0.1 M NaCl, 0.2 mM EDTA, pH 5.5, in 100% $D_2O$, and all the NMR spectra were recorded at 25°C.

### 2.2. NMR spectroscopy

A 2D ($^{13}C$,$^1H$) 70 ms CT-HSQC spectrum was recorded on a Varian VXR 500 Mz spectrometer using a standard pulse sequence [20]. The data were collected with sweep widths of 3100 and 4000 Hz over 216 and 2048 complex points in the $t_1$ ($^{13}C$) and $t_2$ ($^1H$) frequency dimensions, respectively, with quadrature detection in $t_1$ employing the TPPI-States method [21]. A 3.1 ms delay was used to allow heteronuclear antiphase magnetization to evolve and refocus before and after the 70 ms constant time delay. Broadband $^{13}C$ WALTZ decoupling was applied during the $t_2$ acquisition period, and 224 scans were collected per $t_1$ increment, for a total acquisition time of 56 h. The $t_1$ dimension was linear predicted to 512 complex points, multiplied by a 90° shifted skewed (0.5) sine bell window function and zero filled to 4096 complex points; the $t_2$ dimension was zero filled to 16384 complex points and multiplied by a 0.3 Hz line broadening function, prior to Fourier transformation.

A set of spin-echo difference 2D ($^{13}C$,$^1H$) CT-HSQC spectra were recorded with the pulse sequence described by Bax and co-workers [14] except that their $^{15}N$ decoupling pulses were replaced by $^{31}P$ decoupling pulses and no selective or spin lock pulses were used. The experiment was recorded at two constant times, 22 and 44 ms, and for each constant time period two 2D spectra were recorded, a $^{31}P$ coupled and a $^{31}P$ decoupled spectrum [14]. These spectra were acquired on a Varian UnityPlus 500 MHz spectrometer. A 3.0 ms delay was used to allow heteronuclear antiphase magnetization to develop and refocus before and after the 22 or 44 ms constant time period. Broadband $^{13}C$ GARP decoupling was applied during the $t_2$ acquisition period, and quadrature detection in $t_1$ employed the TPPI-States method [21]. For the 22 ms constant time experiment sweep widths of 4000 and 5000 Hz over 87 and 1024 complex points were used in the $t_1$ ($^{13}C$) and $t_2$ ($^1H$) frequency dimensions, respectively, and 192 scans were collected per $t_1$ increment. For each $t_1$ increment a $^{31}P$ decoupled and $^{31}P$ coupled experiment were collected and stored separately for a total acquisition time of 34 h. The same experimental setup was used for the 44 ms constant time experiment except that 155 and 1024 complex points were collected in the $t_1$ ($^{13}C$) and $t_2$ ($^1H$) frequency dimensions, respectively, and 64 scans were collected per transient for a total acquisition time of 20 h. For the 22 ms constant time experiment, the $t_1$ dimension was linear predicted to 256 complex points, zero filled to 1024 complex points, and multiplied by a 90° shifted skewed (0.5) sine bell and a 6 Hz line broadening function, and the $t_2$ dimension was zero filled to 4096 complex points and multiplied by a 3 Hz line broadening function prior to Fourier transformation. For the 44 ms constant time experiment, the $t_1$ dimension was linear predicted to 512 complex points, zero filled to 1024 complex points, and multiplied by a 90° shifted skewed (0.5) sine bell and a 6 Hz line broadening function and the $t_2$ dimension was zero filled to 4096 complex points and multiplied by a 3 Hz line broadening function prior to Fourier transformation. All the data processing was performed on a Silicon Graphics Indigo2 computer using FELIX 2.3 (Biosym Inc.).


*SSDI* 0014-5793(95)00232-4

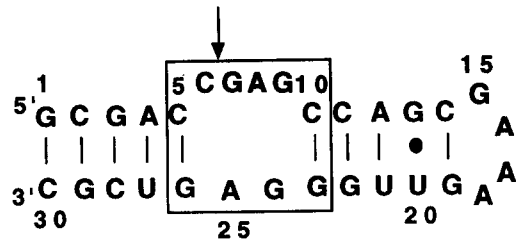


Fig. 1. Schematic representation of the sequence and secondary structure of the leadzyme [15]. The box encloses the nucleotides required for cleavage and the arrow points to the cleavage site.

*2.3. Data analysis*

The percentage of the relative signal intensity difference between the $^{31}P$ decoupled and $^{31}P$ coupled spectra, $\Delta S$, was calculated for the spin-echo difference CT-HSQC spectra using the equation

$$\Delta S(\%) = [(S_d - S_c)/S_d] \times 100$$

where $S_d$is the signal intensity of a 1D cross-section of an individual crosspeak in the $^{31}P$ decoupled spectrum and $S_c$ is the corresponding intensity measurement of the same crosspeak in the $^{31}P$ coupled spectrum. The errors for the relative signal intensities, $\Delta\Delta S$, were based on a statistical analysis of the $\Delta S$ values for the H1′ signal intensities (where $\Delta S$ should be zero), or from the error on the $\Delta S$ values measured on three 1D cross-sections per crosspeak, whichever had the largest value. The ranges of $^3J_{CP}$ were calculated for all 2′ crosspeaks and for the terminal G1 and C30 4′ crosspeaks, using the equation:

$$^3J_{CP}(Hz) = [\cos^{-1}(1-(\Delta S \pm \Delta\Delta S)/100)]/(\pi CT)$$

where CT is the constant time period. The two $^3J_{CP}$ coupling constant values for each non-terminal 4′ crosspeak (referred to as $J_1$ and $J_2$ where $J_2 \geq J_1$) were determined as follows. The range of $J_1$ is $0 \leq J_1 \leq J_2$ and $J_1 \leq J_2 \leq J_{max}$. If $J_1 = 0$ then $J_2 = J_{max}$ and:

$$J_2(Hz) = [\cos^{-1}(1-(\Delta S + \Delta\Delta S)/100)]/(\pi CT)$$

If $J_1 = J_2$, then:

$$J_1(Hz) = [\cos^{-1}(\pm\sqrt{(1-(\Delta S + \Delta\Delta S)/100)})]/(\pi CT) \text{ and}$$

$$J_2(Hz) = [\cos^{-1}(\pm\sqrt{(1-(\Delta S - \Delta\Delta S)/100)})]/(\pi CT)$$

The spin-echo difference CT-HSQC spectra were used to calculate $\Sigma\,^3J_{CP}$, which is the sum of $J_1$ and $J_2$. The minimum for $\Sigma\,^3J_{CP}$, $\Sigma_{min}$, is when $J_1 = 0$ and $J_2 = J_{max}$, and is calculated as:

$$\Sigma_{min} = [\cos^{-1}(1-(\Delta S - \Delta\Delta S)/100)]/(\pi CT).$$

The maximum for $\Sigma\,^3J_{CP}$, $\Sigma_{max}$, is when $J_1 = J_2$ and is calculated as:

$$\Sigma_{max} = 2[\cos^{-1}(\pm\sqrt{(1-(\Delta S + \Delta\Delta S)/100)})]/(\pi CT)$$

where only the larger of the two possible solutions was retained.

## 3. Results and discussion

The structure of a RNA is defined by 6 backbone torsion angles ($\alpha$–$\zeta$) and the glycosidic angle $\chi$) [22]. The glycosidic angle and the sugar pucker ($\delta$) can be well-defined from proton–proton NOE data, but other parts of the backbone are more difficult to define [23]. Thus when generating three-dimensional structures of RNA it is important to obtain J coupling constant data to constrain the backbone torsion angles. $^3J_{HH}$ and $^3J_{HP}$ coupling constants obtained from DQF-COSY and HETCOR experiments are routinely used for structure determination of nucleic acids [2,13]. However, the accurate measurement of J coupling constants from these COSY-type spectra is limited due to problems arising when the linewidths have similar magnitudes to the coupling constants in a crosspeak [12]. This problem can sometimes be overcome in E. COSY-type spectra [24], and analysis of E. COSY patterns in 2D ($^{13}C$,$^1H$) CT-HSQC spectra have been used to measure $^3J_{CP}$ couplings in DNA [25]. This technique is more limited in $^{13}C$,$^{15}N$ labeled RNA, as seen in the CT-HSQC spectrum of the 99% $^{13}C$ labeled leadzyme in Fig. 2. First, the high resolution in the $^{13}C$ dimension required for accurate measurement of these coupling constants demands a long constant time period, but relaxation during the constant time period substantially reduced the signal-to-noise and many crosspeaks were extremely weak or not observed at a constant time period of 70 ms in the leadzyme (see Fig. 2). Second, extracting accurate $^3J_{CP}$ coupling constants from the spectrum in Fig. 2 requires that either $^3J_{CP}$ is much larger than the $^{13}C$ linewidth, and the J coupling can then be obtained from the COSY-type pattern, or that $^4J_{HP}$ is much larger than the $^1H$ linewidth, and the J coupling constant can then be obtained from the E. COSY pattern. Unfortunately in $^{13}C$ labeled RNA, $^3J_{CP}$ is often less than the $^{13}C$ linewidth and $^4J_{HP}$ is less than the $^1H$ linewidth. As illustrated in Fig. 2B, an estimate of the $^3J_{CP}$ coupling constant for

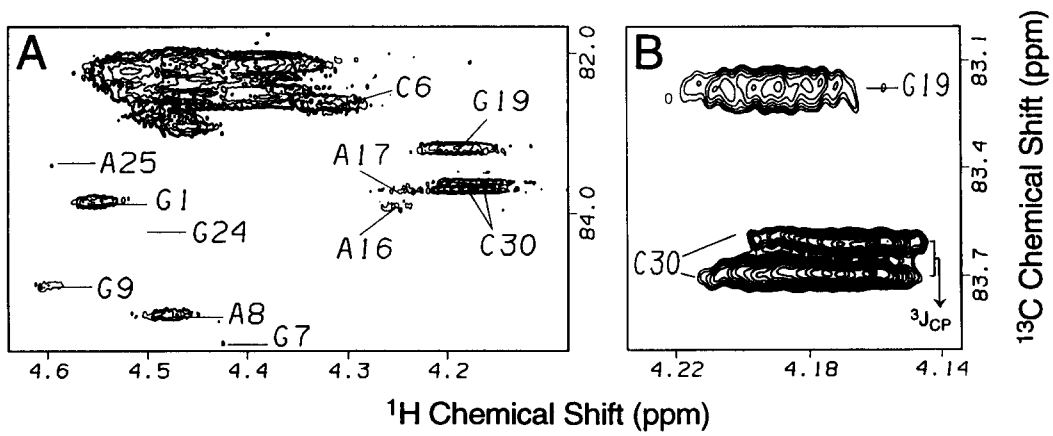


Fig. 2. (A) Contour plot of the 4′ region of the 70 ms ($^{13}C$,$^1H$) CT-HSQC spectrum [20,25] of the leadzyme. Only the well-resolved signals are labeled. Weak and absent crosspeaks are labeled for the purpose of comparing this spectrum with the spectrum presented in Fig. 3A. (B) Expansion of part of the spectrum shown in Fig. 2A.

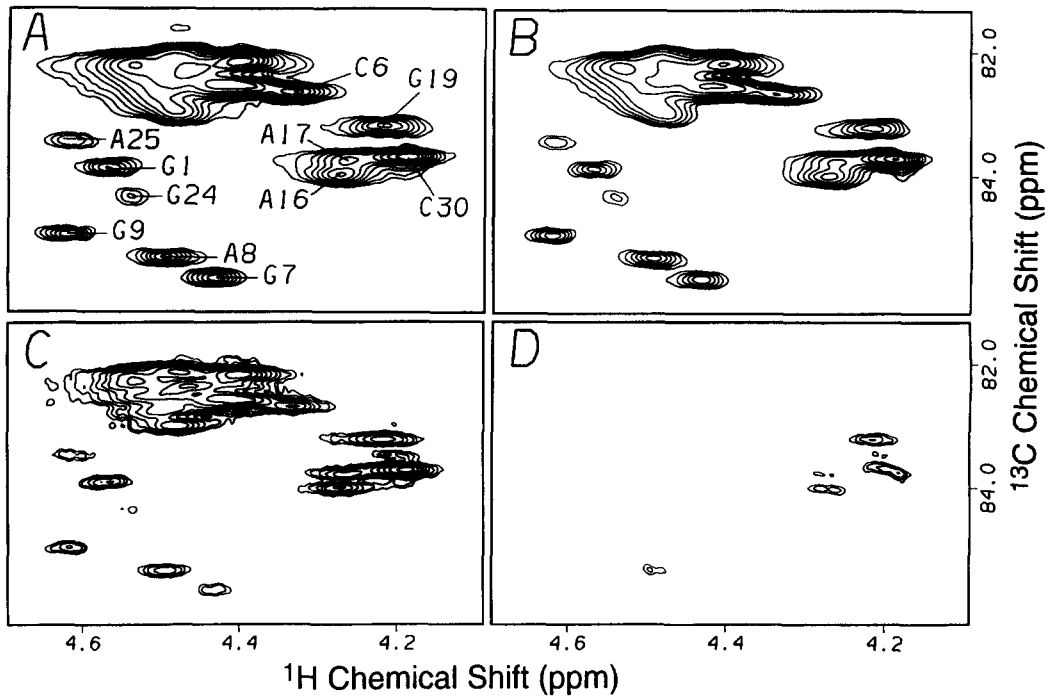


Fig. 3. Contour plot of the 4′ region of the 2D ($^{13}C$,$^{1}H$) (A) $^{31}P$ decoupled 22 ms, (B) $^{31}P$ coupled 22 ms, (C) $^{31}P$ decoupled 44 ms, and (D) $^{31}P$ coupled 44 ms, spin-echo difference CT-HSQC spectra of the leadzyme. Only the well-resolved signals are labeled in A. All crosspeaks shown in the 22 ms spectra have negative intensities and all crosspeaks shown in the 44 ms spectra have positive intensities.

C30 could be extracted in the $^{13}C$ dimension from the COSY-type pattern of this crosspeak. However, most other residues had crosspeak patterns such as that observed for G19 in Fig. 2B, from which it was impossible to obtain useful coupling constant data.

To overcome these problems a set of triple resonance spin-echo difference 2D ($^{13}C$,$^{1}H$) CT-HSCQ spectra [14] were acquired on the leadzyme. In these spectra the magnitude of the J coupling can be calculated from comparison of the intensity of a crosspeak in the spectra with and without $^{31}P$ decoupling during the constant time period [14]. Because intensities are measured, the signal-to-noise, not the linewidth, is the limiting factor in analysis of the J coupling constants.

Fig. 3 shows contour plots of the 4′ region of the spin-echo difference CT-HSQC spectra with and without $^{31}P$ decoupling. These spectra were recorded at 22 and 44 ms constant time periods because the constant time period must be a multiple of $1/J_{CC}$, where $J_{CC}$ = 42–45 Hz. There is a slight decrease in intensity in the $^{31}P$ coupled spectrum (Fig. 3B) compared to the $^{31}P$ decoupled spectrum (Fig. 3A) at 22 ms. The corresponding difference is much larger at 44 ms (Fig. 3D and C) where most of the crosspeaks disappear in the $^{31}P$ coupled spectrum. These

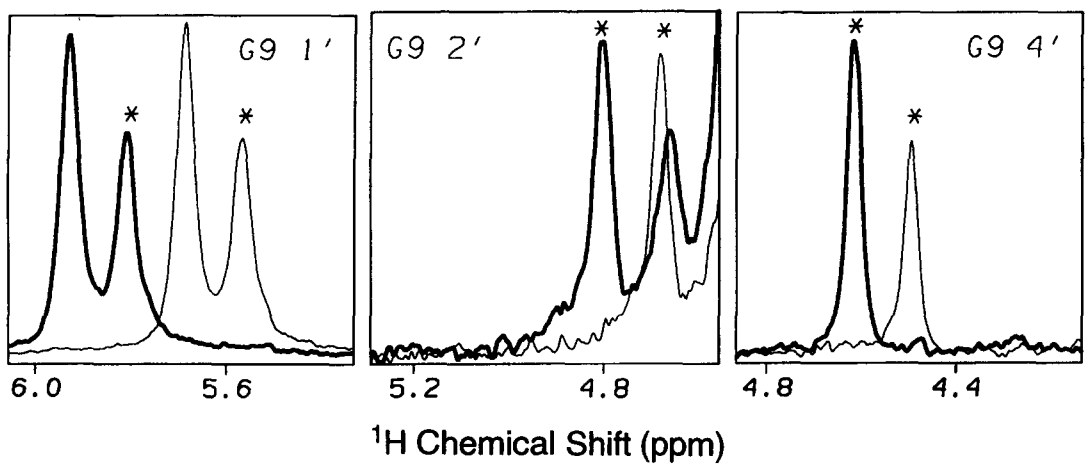


Fig. 4. 1D cross-sections for G9 1′, 2′, and 4′ crosspeaks of the 22 ms spin-echo difference ($^{13}C$,$^{1}H$) CT-HSQC spectra presented in Fig. 3 with (thick line) and without (thin line) $^{31}P$ decoupling. The spectra without $^{31}P$ decoupling are offset to illustrate the intensity differences. The peaks for residue G9 are marked with an asterisk. Since the 4′ peaks have the opposite sign to the 1′ and 2′ peaks, they were multiplied by −1 to facilitate the representation. The signal-to-noise is an important factor in how precisely the J coupling constants can be measured by this technique. As a reference, the signal-to-noise of the 1D cross-sections of the $^{31}P$ decoupled spectra for the G9 1′, 2′, and 4′ are 75:1, 35:1 and 35:1, respectively.

differences reflect the principle behind measuring coupling constants by this technique. In the $^{31}P$ coupled experiment the intensity of a resonance with a single $J_{CP}$ coupling is modulated by $\cos(\pi J_{CP}CT)$, whereas in the $^{31}P$ decoupled experiment, there is no modulation of the signal intensity during the constant time period [14].

Fig. 4 shows pairs of 1D cross-sections from the 22 ms spin-echo difference CT-HSQC spectra with and without $^{31}P$ decoupling for the G9 1′, 2′, and 4′ crosspeaks. The intensities of the 1′ resonances are the same in both spectra because the 1′ carbons are not coupled to any $^{31}P$. The C1′ crosspeaks therefore serve as excellent controls and were used to estimate errors in the measurement of signal intensities of other crosspeaks (data not shown). As seen in Fig. 4, measurable differences in the intensity of individual crosspeaks were observed between the $^{31}P$ coupled and the $^{31}P$ decoupled spectra for the 2′ and 4′ resonances, demonstrating that these carbons are coupled to at least one $^{31}P$.

Table 1 lists the $^3J_{C2'P}$ and $^3J_{C4'P}$ coupling constants that were measured for the leadzyme. It is clear from these data that the

Table 1
$^3J_{CP}$ coupling data for the $^{13}C,^{15}N$ labeled leadzyme[a]

| Cross-peak | ΔS (%) in the 22 ms spin-echo difference CT-HSQC (Fig. 3A,B) | ΔS (%) in the 44 ms spin-echo difference CT-HSQC (Fig. 3C,D) | Range of $^3J_{CP}$ (Hz) in the 22 ms spin-echo difference CT-HSQC (Fig. 3A,B) | Range of $^3J_{CP}$ (Hz) in the 44 ms spin-echo difference CT-HSQC (Fig. 3C,D) | Range of $^3J_{CP}$ (Hz) from peak separation in the 70 ms CT-HSQC[b] (Fig. 2) | Minimal range of $^3J_{CP}$ (Hz)[c] |
|---|---|---|---|---|---|---|
| G1 2′ | −2 ± 5 | too weak[d] | ≤3.6 | too weak | too weak | ≤3.6 |
| C6 2′ | 0 ± 3 | −2 ± 7 | ≤3.6 | ≤2.3 | ≤3.6 | ≤2.3 |
| G9 2′ | −1 ± 6 | 14 ± 10 | ≤4.6 | 2.1–5.1 | ≤4.5 | 2.1–4.5 |
| A12 2′ | 2 ± 8 | 12 ± 10 | ≤6.5 | 1.4–4.9 | ≤4.6 | 1.4–4.6 |
| C14 2′ | 0 ± 3 | 1 ± 5 | ≤3.6 | ≤2.5 | ≤4.4 | ≤2.5 |
| G15 2′ | 3 ± 6 | 0 ± 5 | ≤6.2 | ≤2.3 | ≤4.5 | ≤2.3 |
| A16 2′ | 5 ± 3 | 2 ± 9 | 2.9–5.8 | ≤3.4 | ≤4.4 | 2.9–3.4 |
| A17 2′ | 3 ± 4 | too weak | ≤5.4 | too weak | too weak | ≤5.4 |
| A18 2′ | −2 ± 4 | 4 ± 10 | ≤2.9 | ≤3.9 | ≤4.5 | ≤2.9 |
| G19 2′ | −2 ± 3 | −14 ± 20 | ≤2.0 | ≤2.5 | too weak | ≤2.0 |
| U20 2′ | 2 ± 3 | 0 ± 10 | ≤4.6 | ≤3.3 | ≤4.4 | ≤3.3 |
| A25 2′ | 5 ± 3 | −13 ± 22 | 2.9–5.8 | ≤3.1 | ≤4.3 | 2.9–3.1 |
| C30 2′ | 0 ± 3 | −3 ± 5 | ≤3.6 | ≤1.4 | ≤1.7 | ≤1.4 |
| G1 4′ | 28 ± 3 | 81 ± 10 | 10.5–11.7 | 9.2–10.7 | 8.0–12.0 | 10.5–10.7 |
| C6 4′ | 35 ± 3 | 94 ± 10 | $J_1$ = ≤9.6<br>$J_2$ = 8.7–13.1<br>11.9 ≤ Σ ≤ 19.2[f] | $J_1$ = ≤11.7<br>$J_2$ = 8.4–11.7<br>10.2 ≤ Σ ≤ 23.4 | too complex[e] | $J_1$ = ≤9.6<br>$J_2$ = 8.7–11.7<br>10.2 ≤ Σ ≤ 19.2 |
| G7 4′ | 23 ± 3 | 100 ± 50 | $J_1$ = ≤7.7<br>$J_2$ = 6.7–10.7<br>9.3 ≤ Σ ≤ 15.4 | $J_1$ = ≤15.2<br>$J_2$ = 5.7–15.2<br>7.6 ≤ Σ ≤ 30.4 | too weak | $J_1$ = ≤7.7<br>$J_2$ = 6.7–10.7<br>9.3 ≤ Σ ≤ 15.4 |
| A8 4′ | 21 ± 6 | 64 ± 10 | $J_1$ = ≤7.9<br>$J_2$ = 5.8–10.9<br>8.0 ≤ Σ ≤ 15.8 | $J_1$ = ≤7.5<br>$J_2$ = 6.0–9.5<br>7.9 ≤ Σ ≤ 15.0 | Σ ≤ 19 | $J_1$ = ≤7.5<br>$J_2$ = 6.0–9.5<br>7.9 ≤ Σ ≤ 15.0 |
| G9 4′ | 30 ± 4 | 84 ± 16 | $J_1$ = ≤9.0<br>$J_2$ = 7.7–12.3<br>10.7 ≤ Σ ≤ 18.0 | $J_1$ = ≤11.4<br>$J_2$ = 7.0–11.4<br>9.0 ≤ Σ ≤ 22.8 | too weak | $J_1$ = ≤9.0<br>$J_2$ = 7.7–11.4<br>9.0 ≤ Σ ≤ 18.0 |
| A16 4′ | 19 ± 3 | 61 ± 10 | $J_1$ = ≤7.1<br>$J_2$ = 6.0–9.8<br>8.3 ≤ Σ ≤ 14.2 | $J_1$ = ≤7.3<br>$J_2$ = 5.8–9.2<br>7.7 ≤ Σ ≤ 14.6 | too weak | $J_1$ = ≤7.1<br>$J_2$ = 6.0–9.2<br>7.7 ≤ Σ ≤ 14.2 |
| A17 4′ | 29 ± 3 | 74 ± 10 | $J_1$ = ≤8.7<br>$J_2$ = 7.7–11.9<br>10.7 ≤ Σ ≤ 17.4 | $J_1$ = ≤8.4<br>$J_2$ = 6.7–10.2<br>8.7 ≤ Σ ≤ 16.8 | too weak | $J_1$ = ≤8.4<br>$J_2$ = 7.7–10.2<br>8.7 ≤ Σ ≤ 16.8 |
| A19 4′ | 20 ± 3 | 69 ± 10 | $J_1$ = ≤7.2<br>$J_2$ = 6.1–10.0<br>8.6 ≤ Σ ≤ 14.4 | $J_1$ = ≤7.9<br>$J_2$ = 6.3–9.8<br>8.3 ≤ Σ ≤ 15.8 | Σ ≤ 20 | $J_1$ = ≤7.2<br>$J_2$ = 6.3–9.8<br>8.3 ≤ Σ ≤ 14.4 |
| G24 4′ | 23 ± 3 | too weak | $J_1$ = ≤7.7<br>$J_2$ = 6.7–10.7<br>9.3 ≤ Σ ≤ 15.4 | too weak | too weak | $J_1$ = ≤7.7<br>$J_2$ = 6.7–10.7<br>9.3 ≤ Σ ≤ 15.4 |
| A25 4′ | 35 ± 3 | 100 ± 37 | $J_1$ = ≤9.6<br>$J_2$ = 8.7–13.1<br>11.9 ≤ Σ ≤ 19.2 | $J_1$ = ≤14.1<br>$J_2$ = 6.6–14.1<br>8.6 ≤ Σ ≤ 28.2 | too weak | $J_1$ = ≤9.6<br>$J_2$ = 8.7–13.1<br>11.9 ≤ Σ ≤ 19.2 |
| C30 4′ | 30 ± 3 | 86 ± 10 | 10.9–12.1 | 9.6–11.1 | 9.0–13.0 | 10.9–11.1 |

[a] Only data from the resolved 2′ and 4′ crosspeaks were obtained. See section 2.3 for measurement of signal intensities, calculation of the relative signal intensity difference (ΔS), calculation of $^3J_{CP}$ (Hz) from ΔS in the 22 and 44 ms spin-echo difference CT-HSQC spectra ($J_1$, $J_2$, and Σ $^3J_{CP}$), and complete error analysis.
[b] Ranges for the individual $^3J_{CP}$ coupling constants obtained from the analysis of peak separation in the 70 ms CT-HSQC spectrum.
[c] The minimal ranges for $^3J_{CP}$ were obtained by combining all the data from the 22 and 44 ms spin-echo difference CT-HSQC spectra and the 70 ms CT-HSQC spectrum.
[d] The peak is too weak to analyze.
[e] The peak has too complex a splitting pattern to analyze.
[f] Here Σ represents Σ $^3J_{CP}$.

spin-echo difference spectra provided much more J coupling constant information than the 70 ms CT-HSQC spectrum. As discussed above, many $^3J_{CP}$ coupling constants obtained in the spin-echo difference spectra could not be extracted from the 70 ms CT-HSQC spectrum. For the $^3J_{CP}$ coupling constants that could be measured by both techniques, in every case, the data from the spin-echo difference spectra led to more precisely defined $^3J_{CP}$ coupling constants than data from the 70 ms CT-HSQC spectrum.

The $^3J_{CP}$ coupling constants that are most useful for structure determination of RNAs are $^3J_{C2'P}$ and $^3J_{C4'P}$. The $^3J_{C2'P}$ coupling constants give information on the $\varepsilon$ torsion angle and the $^3J_{C4'P}$ coupling constants give information on the $\beta$ and $\varepsilon$ torsion angles [13]. The $^3J_{C2'P}$ coupling constants were used to restrict the conformation of the $\varepsilon$ torsion angle through the Karplus relation [13]. All of the $^3J_{C2'P}$ coupling constants observed in the leadzyme (see Table 1) were small ($\leq 5.4$ Hz) which restricts this angle to the $g^+$ and t conformations. However, the $g^+$ conformation for $\varepsilon$ is not common in nucleic acids and is energetically unfavorable [26]. Thus the $^3J_{C2'P}$ coupling constants derived from these spin-echo difference CT-HSQC spectra yielded valuable $\varepsilon$ torsion angle constraints for the leadzyme.

Extracting $^3J_{CP}$ coupling constants from the 4′ crosspeaks is more complicated than for the 2′ crosspeaks since for the non-terminal residues, each C4′ is coupled to two $^{31}P$. As seen in Table 1, the $^3J_{C4'P}$ coupling constants for the two terminal residues, G1 and C30, were very precisely determined from the spin-echo difference CT-HSQC spectra. For many non-terminal residues, it was possible to calculate ranges for the two individual $^3J_{C4'P}$ coupling constants, and ranges for their sums, $\Sigma\,^3J_{CP}$ (see Table 1). An interesting case is for residue A16 where the $^3J_{C2'P}$ coupling constant is well defined (2.9–3.4 Hz), which made it possible to assign the two $^3J_{C4'P}$ coupling constants to their specific torsion angles (data not shown). For the other residues the ranges for the $^3J_{C4'P}$ coupling constants, and their sums $\Sigma\,^3J_{CP}$, can be used to restrict the backbone conformation by refining the RNA structure directly against the J coupling constants [27,28].

## 4. Conclusions

The results presented here illustrate that recently developed spin-echo difference CT-HSQC experiments for quantitative measurement of heteronuclear J coupling constants in proteins [14] can be readily applied to isotopically labeled RNAs. The data obtained on the $^{13}C$ labeled leadzyme clearly show that this spin-echo difference technique leads to more precisely defined $^3J_{CP}$ coupling constants than previously used techniques. The precision of a J coupling constant determined by the spin-echo difference CT-HSQC experiment is dictated by the signal-to-noise of the crosspeak and is unaffected by the linewidth of the peak. One limitation of the technique is that J coupling constant information can only be extracted for well resolved crosspeaks in the 2D spectrum. Although the helical regions in RNAs often show significant overlap, the structurally interesting regions of RNAs often show well-resolved spectra, as observed here for the active site internal loop and the $GA_3$ loop of the leadzyme. However, this spectral overlap problem can be overcome by extending this spin-echo difference procedure into a three-dimensional experiment [29]. The additional structural constraints provided by measurement of the three-bond $^{13}C,^{31}P$ coupling constants should prove extremely valuable for solution structure determinations of isotopically labeled RNAs.

*Acknowledgments:* We thank Dr. Evan Williams and Varian Instruments for providing time on their UnityPlus 500 NMR spectrometer. This work was supported by NIH Grants AI30726, AI33098, and a NIH Research Career Development Award AI01051 to A.P. P.L. was supported by a NSERC 1967 Science and Engineering scholarship and a FCAR (Fonds pour la Formation de Chercheurs et l' Aide à la Recherche) scholarship. The VXR-500 MHz NMR spectrometer was purchased with partial support from NIH Grant RR03283. We also thank the W.M. Keck Foundation for their generous support of RNA science on the Boulder campus.

## References

[1] Gesteland, R.F. and Atkins, J.F. (1993) The RNA World, Cold Spring Harbor Laboratory, Plainview, NY.
[2] Varani, G. and Tinoco Jr., I. (1991) Q. Rev. Biophys. 24, 479–532.
[3] Nikonowicz, E.P., Sirr, A., Legault, P., Jucker, F.M., Baer, L.M. and Pardi, A. (1992) Nucleic Acids Res. 20, 4507–4513.
[4] Batey, R.T., Inada, M., Kujawinski, E., Puglisi, J.D. and Williamson, J.R. (1992) Nucleic Acids Res. 20, 4515–4523.
[5] Nikonowicz, E.P. and Pardi, A. (1992) Nature 355, 184–186.
[6] Nikonowicz, E.P. and Pardi, A. (1992) J. Am. Chem. Soc. 114, 1082–1083.
[7] Farmer, B.T., II, Mueller, L., Nikonowicz, E.P. and Pardi, A. (1993) J. Am. Chem. Soc. 115, 11040–11041.
[8] Sklenar, V., Peterson, R.D., Rejante, M.R., Wang, E. and Feigon, J. (1993) J. Am. Chem. Soc. 115, 12181–12182.
[9] Nikonowicz, E.P. and Pardi, A. (1993) J. Mol. Biol. 232, 1141–1156.
[10] Heus, H.A., Wijmenga, S.S., van de Ven, F.J.M. and Hilbers, C.W. (1994) J. Am. Chem. Soc. 116, 4983–4984.
[11] Marino, J.P., Schwalbe, H., Anklin, C., Bermel, W., Crothers, D.M. and Griesinger, C. (1994) J. Am. Chem. Soc. 116, 6472–6473.
[12] Wüthrich, K. (1986) NMR of Proteins and Nucleic Acids, Wiley, New York.
[13] Wijmenga, S.S., Mooren, M.M.W. and Hilbers, C.W. (1993) in: NMR of Macromolecules (G.C.K. Roberts, ed.) pp. 217–288, Oxford University Press, Oxford.
[14] Vuister, G.W., Wang, A.C. and Bax, A. (1993) J. Am. Chem. Soc. 115, 5334–5335.
[15] Pan, T. and Uhlenbeck, O.C. (1992) Nature 358, 560–563.
[16] Legault, P. and Pardi, A. (1994) J. Magn. Reson. Series B 103, 82–86.
[17] Legault, P., Farmer, B.T., Mueller, L. and Pardi, A. (1994) J. Am. Chem. Soc. 116, 2203–2204.
[18] Legault, P. and Pardi, A. (1994) J. Am. Chem. Soc. 116, 8390–8391.
[19] Milligan, J.F., Groebe, D.R., Witherell, G.W. and Uhlenbeck, O.C. (1987) Nucleic Acids Res. 15, 8783–8789.
[20] Santoro, J. and King, G.C. (1992) J. Magn. Reson. 97, 202–207.
[21] Marion, D., Ikura, M., Tschudin, R. and Bax, A. (1989) J. Magn. Reson. 85, 393–399.
[22] Saenger, W. (1984) Principles of Nucleic Acid Structure, Springer-Verlag, New York.
[23] Pardi, A., Hare, D.R. and Wang, C. (1988) Proc. Natl. Acad. Sci. USA 85, 8785–9.
[24] Montelione, G.T. and Wagner, G. (1989) J. Am. Chem. Soc. 111, 5474–5475.
[25] Schmieder, P., Ippel, J.H., van de Nelst, H., van der Marel, G.A., van Boom, J.H., Altona, C. and Kessler, H. (1992) Nucleic Acids Res. 20, 4747–4751.
[26] Mooren, M.M.W. (1993) Ph.D. Thesis, University of Nijmegen, Nijmegen, The Netherlands.
[27] Pearlman, D.A. (1994) J. Biomol. NMR 4, 279–299.
[28] Garrett, D.S., Kuszewski, J., Hancock, T.J., Lodi, P.J., Vuister, G.W., Gronenborn, A.M. and Clore, G.M. (1994) J. Magn. Reson. Series B 104, 99–103.
[29] Vuister, G.W. and Bax, A. (1993) J. Am. Chem. Soc. 115, 7772–7777.